

Long-Lived, Transferred Crystalline Silicon Carbide Nanomembranes for Implantable Flexible Electronics

Hoang-Phuong Phan,^{*,†,‡,§} Yishan Zhong,[‡] Tuan-Khoa Nguyen,[†] Yoonseok Park,[‡] Toan Dinh,^{†,§} Enming Song,^{‡,¶} Raja Kumar Vadivelu,[†] Mostafa Kamal Masud,^{||} Jinghua Li,^{‡,¶,▽} Muhammad J.A. Shiddiky,^{†,○} Dzung Dao,^{†,§} Yusuke Yamauchi,^{||,¶,&} John A. Rogers,^{*,#} and Nam-Trung Nguyen^{*,†}

[†]Queensland Micro and Nanotechnology Centre, Griffith University, Brisbane, Queensland 4111, Australia

[‡]Center for Bio-Integrated Electronics, Northwestern University, Evanston, Illinois 60208, United States

[§]School of Engineering and Built Environment, Griffith University, Gold Coast, Queensland 4215, Australia

[¶]Frederick Seitz Materials Research Laboratory, University of Illinois at Urbana—Champaign, Urbana, Illinois 61801, United States

^{||}Australian Institute for Bioengineering & Nanotechnology and School of Chemical Engineering, University of Queensland, Brisbane, Queensland 4072, Australia

[¶]Department of Materials Science and Engineering, Northwestern University, Evanston, Illinois 60208, United States

[○]School of Environment and Science, Griffith University, Brisbane, Queensland 4111, Australia

[&]International Center for Materials Nanoarchitectonics (WPI-MANA), National Institute for Materials Science (NIMS), 1-1 Namiki, Tsukuba, Ibaraki 305-0044, Japan

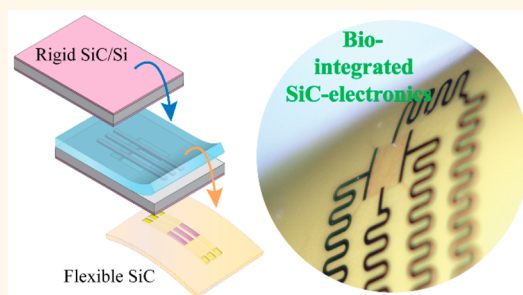
[▽]Department of Plant & Environmental New Resources, Kyung Hee University, 1732 Deogyong-daero, Giheung-gu, Yongin-si, Gyeonggi-do 446-701, Korea

[#]Center for Bio-Integrated Electronics, Department of Materials Science and Engineering, Biomedical Engineering, Chemistry, Mechanical Engineering, Electrical Engineering and, Computer Science, and Neurological Surgery, Simpson Querrey Institute for Nano/biotechnology, McCormick School of Engineering and Feinberg School of Medicine, Northwestern University, Evanston, Illinois 60208, United States

Supporting Information

ABSTRACT: Implantable electronics are of great interest owing to their capability for real-time and continuous recording of cellular–electrical activity. Nevertheless, as such systems involve direct interfaces with surrounding biofluidic environments, maintaining their long-term sustainable operation, without leakage currents or corrosion, is a daunting challenge. Herein, we present a thin, flexible semiconducting material system that offers attractive attributes in this context. The material consists of crystalline cubic silicon carbide nanomembranes grown on silicon wafers, released and then physically transferred to a final device substrate (e.g., polyimide). The experimental results demonstrate that SiC nanomembranes with thicknesses of 230 nm do not experience the hydrolysis process (i.e., the etching rate is 0 nm/day at 96 °C in phosphate-buffered saline (PBS)). There is no observable water permeability for at least 60 days in PBS at 96 °C and non- Na^+ ion diffusion detected at a thickness of 50 nm after being soaked in 1× PBS for 12 days. These properties enable Faradaic interfaces between active electronics and biological tissues, as well as multimodal sensing of temperature, strain, and other properties without the need for additional encapsulating layers. These findings create important opportunities for use of flexible, wide band gap materials as essential components of long-lived neurological and cardiac electrophysiological device interfaces.

KEYWORDS: implantable electronics, flexible electronics, silicon carbide, long-lived operation, neuro-electrophysiology, multifunctional sensing



Due to recent advances in biocompatible, flexible electronics, implantable sensing systems have emerged as an important technology for electrophysiological recording and stimulation. The use of implantable electronics

Received: July 1, 2019

Accepted: August 21, 2019

Published: August 21, 2019

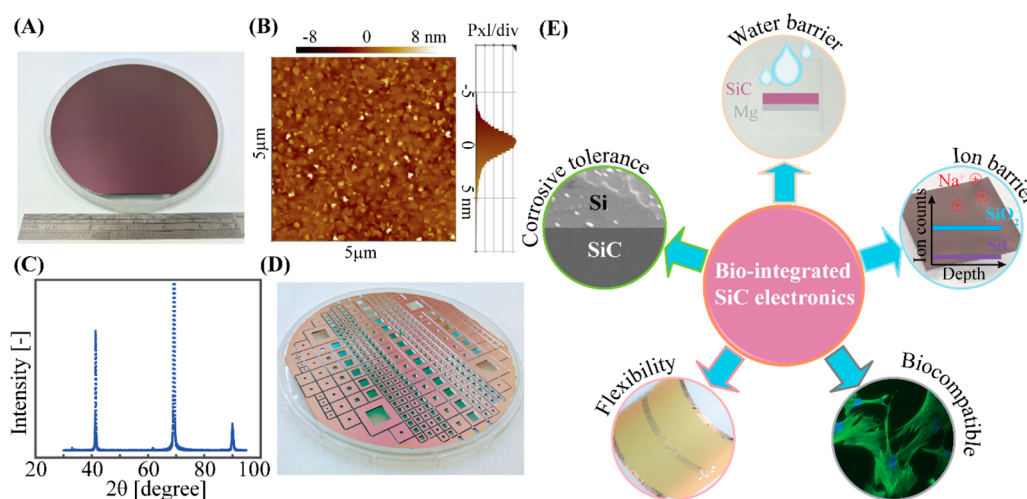


Figure 1. Cubic SiC materials for long-lived implantable electronics. (A) Photograph of a film of SiC grown on a 6 in. Si substrate. (B) AFM data collected from a $5\ \mu\text{m} \times 5\ \mu\text{m}$ area of the as-grown SiC film. (C) XRD θ – 2θ scan on the SiC/Si wafer. (D) Wafer level fabrication of free-standing SiC nanomembranes where a SiC layer grown on the back side of Si was utilized as the hard mask for Si wet-etching. (E) Generic concept for SiC electronics in long-lived implantable applications.

could enable real-time, continuous monitoring of cellular and tissue level activities, providing valuable information for diagnosis and treatment of neurological disorders or cardiac diseases.^{1–5} For instance, silicon nanomembrane transistors in flexible substrates serve as the foundations for electronics capable of multiplexed, *in vivo* recording of cardiac electrophysiology with minimal invasive interfaces, owing to mechanical and geometrical matching to soft, curved, and moving biological tissues.⁶ In some cases, sensing combines with stimulation to provide closed-loop feedback control over organ function, such as in the case of strain gauges and optogenetic interfaces to the bladder expansion to normalize overactive urination.⁷ In applications such as deep brain stimulators (*e.g.*, brain–machine interface) and cardiac pacemakers, a relevant operational time frame for the devices corresponds to the life of the patient. For systems designed with robust engineering margins, the desired lifetime might be more than 100 years.⁸ In this context, the development of submicron layers as robust barriers to biofluid penetration represents one of the most significant material challenges. Silicon itself dissolves in aqueous environments by hydrolysis under physiological conditions,^{9–11} thereby demanding the integration of separate layers for encapsulation.^{12–16} Silicon dioxide, thermally grown on device-grade silicon wafers, represents an excellent choice due to its relative impermeability to water and its low rate of hydrolysis compared to that of Si.^{12–14} Nevertheless, SiO₂ layers for multidecade lifetimes require thicknesses of a few hundred nanometers, thereby leading to relatively low capacitive coupling for sensing and/or stimulation.¹⁴ More generally, full coverage of SiO₂ on the electronics prevents the formation of Faradaic bioelectrical interfaces, thereby hindering applications that require direct electrical contact. Recent reports describe the use of highly doped p⁺-Si and Si/TiSi₂ *via* structures as strategies that circumvent these limitations.^{17,18} However, the complexity of the resulting structures and the inability to exploit semiconducting interfaces for photothermal effects, photoelectronics, piezoresistive/piezoelectric responses, and photoacoustic phenomena could hinder other potentially interesting modalities for measurements of intracellular and extracellular pathways.^{19–22}

Here, we introduce the use of physically transferred nanomembranes of single-crystalline silicon carbide (SiC) on flexible substrates as excellent biofluid barriers that offer semiconducting functionality and long-lived stability under immersion in simulated biofluids. Owing to its chemical inertness and stable electrical properties, SiC electronic interfaces can operate in biofluid environments without any encapsulation layers. We note that silicon carbide has been extensively investigated for harsh environmental applications including high temperatures (*e.g.*, in the combustion engines of automobiles),^{23–26} mechanically/chemically corrosive conditions (*e.g.*, in gas/oil transporting pipeline systems),^{27–29} and high radiation environments (*e.g.*, in space exploration missions).^{30,31} However, as conventional SiC electronics devices require rigid substrates, strongly mismatched to the properties of soft biotissues, the potential of these materials for flexible implantable electronics has been rarely reported.^{32–35} In recent studies, by employing the low deposition temperatures, amorphous SiC grown directly on polymers or metals has been utilized as a protective layer for flexible neural electrodes.^{36,37} As amorphous SiC is generally associated with a high density of defects (*e.g.*, point defects, and dangling bonds) and pinholes, hydrolysis and diffusion processes can occur in these films,³⁶ with the potential to lead to device failure. In addition, due to its low electrical conduction, applications of amorphous SiC are typically limited to biobarriers but not as sensing elements or active device components. Single-crystalline SiC is preferred to amorphous SiC for electrodes and sensing applications owing to its high conductance and its capability of integrating with other electronics devices (*e.g.*, transistors and diodes). Bernadin *et al.* utilized single-crystalline 4H-SiC as neural recording electronics.³⁸ Nevertheless, due to the chemical inertness of 4H-SiC, releasing free-standing thin 4H-SiC films from bulk wafers was not possible. Beygi *et al.* developed a thick p–n junction in cubic SiC for neural interfaces; however, as the thickness of the film was relatively large (8 μm), this platform was only suitable for the shank configuration.³⁹ To date, a flexible single-crystalline SiC platform for biosensing and recording applications has not been realized. This work develops and elucidates the long-term stability and multifunctionality of nanomembrane crystalline SiC flexible electronics, as oppor-

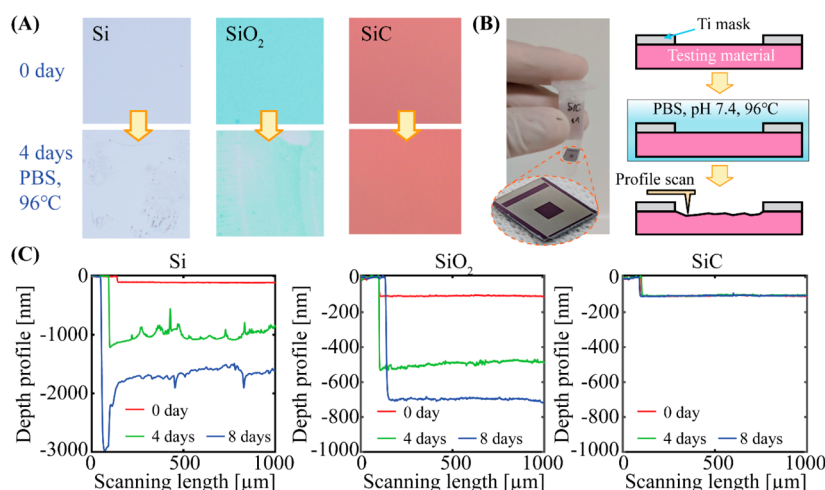


Figure 2. Rate of hydrolysis of SiC in comparison to other encapsulation materials. (A) Colorimetric indication of changes in thickness and/or surface morphology due to hydrolysis from soaking in PBS at pH 7.4 and 96 °C for 4 days. (B) Image of the devices used in determining etching depth by profile scanning. (C) Quantification of the hydrolysis of Si, PECVD oxide, thermal oxide, and SiC.

tunities for applications in long-lived cellular monitoring, recording, and stimulation.

RESULTS AND DISCUSSION

The silicon carbide nanomembranes were fabricated following the growth of nanoscale films on silicon wafers using low-pressure chemical vapor deposition (LPCVD).^{40,41} To balance the residual stress in the SiC films due to high-temperature CVD process, we deposited SiC films on both sides of the silicon wafers, helping to avoid large wafer bowing and cracking. Among numerous SiC polytypes, such as hexagonal (4H-SiC and 6H-SiC) and cubic (3C-SiC) crystals, our material of choice is 3C-SiC as this is the only crystal that can be grown on a Si substrate, making it compatible with conventional MEMS fabrication technologies as well as reducing material cost.^{42,43} Figure 1A shows a photograph of an as-deposited 6 in. SiC/Si wafer where the thickness of the SiC is 230 nm. The atomic force microscopy (AFM) data show excellent surface smoothness with a root mean square roughness of less than 3 nm (Figure 1B), with a thickness uniformity of less than $\pm 1\%$. The X-ray diffraction (XRD) pattern shows obvious peaks at 41.1 and 90° (*i.e.*, 2θ) corresponding to SiC(100), whereas the peak at 69.1° is derived from the Si substrate (Figure 1C). The results confirm that the SiC films are epitaxially deposited on Si, with crystallographic orientation aligned with that of the substrate. The conductivity of SiC can be tuned by *in situ* introduction of dopants (*e.g.*, Al or N) during the deposition process, making it possible to form either p-type or n-type SiC. Figure 1D demonstrates the capability for full wafer-scale level fabrication of the SiC/Si platform, in which the SiC layer deposited on the backside of Si was utilized to form free-standing SiC nanomembranes (with dimensions varying from 300 $\mu\text{m} \times 300 \mu\text{m}$ up to 10 mm \times 10 mm). Figure 1E illustrates desirable properties in SiC for long-lived implantable electronics, including (i) low hydrolysis rate, (ii) impermeability to water, (iii) low ion diffusivity, (iv) biocompatibility, and (v) mechanical flexibility, as elucidated in the following experiments.

The hydrolysis rate for SiC was investigated by soaking the as-deposited SiC-on-Si film into phosphate-buffered saline (PBS, pH 7.4) at 96 °C. The soak test in PBS solution was performed at an increased temperature (instead of a physiological temperature, 37 °C) as an accelerated test for long-term operation (*e.g.*,

the bilayer 100 nm HfO₂/100 nm SiO₂ that can withstand PBS at 96 °C for 10 days is expected to last for more than 50 years at human body temperature using the Arrhenius approximation: lifetime $\propto \exp(E_a/K_B T)$, where E_a is the activation energy (*i.e.*, 1.32 eV for the case of SiO₂), K_B is the Boltzmann constant, and T is the testing temperature).¹² As the hydrolysis process changes the thicknesses and/or surface morphologies of the films, the effects can be readily detected by optical observation with the naked eye or under a microscope. Figure 2A shows optical images of p⁺⁺ Si (boron-doped, sourced University Wafer), thermal oxide, and SiC films before and after 4 days of immersion in PBS at 96 °C. The changes in the surface roughness of Si and reflected color of SiO₂/Si are consistent with expected rates of hydrolysis in these materials. On the other hand, no significant colorimetric change occurs in the as-deposited SiC nanothin film, indicating the stability of this semiconductor material. To further quantify the hydrolysis phenomenon in the as-grown SiC film, we patterned Ti windows as hard masks on the SiC surface and measured the film thickness using a scanning surface profiler (Dektak 150) (Figure 2B). Figure 2C shows profile scans and the etching rate after 0, 4, and 8 days of Si, thermal oxide, and SiC. These results clearly indicate that the thickness of the SiC films remains constant throughout this period. Soaking the SiC samples in PBS for 30 days under these same conditions also leads to a negligible change in thickness of the films. For Si (heavily doped with boron) and thermal SiO₂, the dissolution rates are 200 and 80 nm/day at 96 °C, respectively. Figures S3 and S4 further demonstrate the chemical inertness of SiC nanomembranes in different chemical solutions.

To explore the water barrier function of SiC, we employed magnesium (Mg) deposited on free-standing SiC nanomembranes as a sensing layer to determine the time scale for water diffusion through the SiC (Figure 3A). The aggressive hydrolysis process for magnesium ($\text{Mg} + 2\text{H}_2\text{O} = \text{Mg}(\text{OH})_2 + \text{H}_2$) rapidly changes the surface morphology of the Mg film to provide an immediate visual indication of water penetration (Figure 3B). Generally, the water diffusion is accelerated by the hydrolysis process (which thins the barrier layer such as thermal oxide), direct permeation through the material, or the existence of pinholes or other defects that allow water molecules to rapidly penetrate through.¹⁴ The former possibility can be eliminated

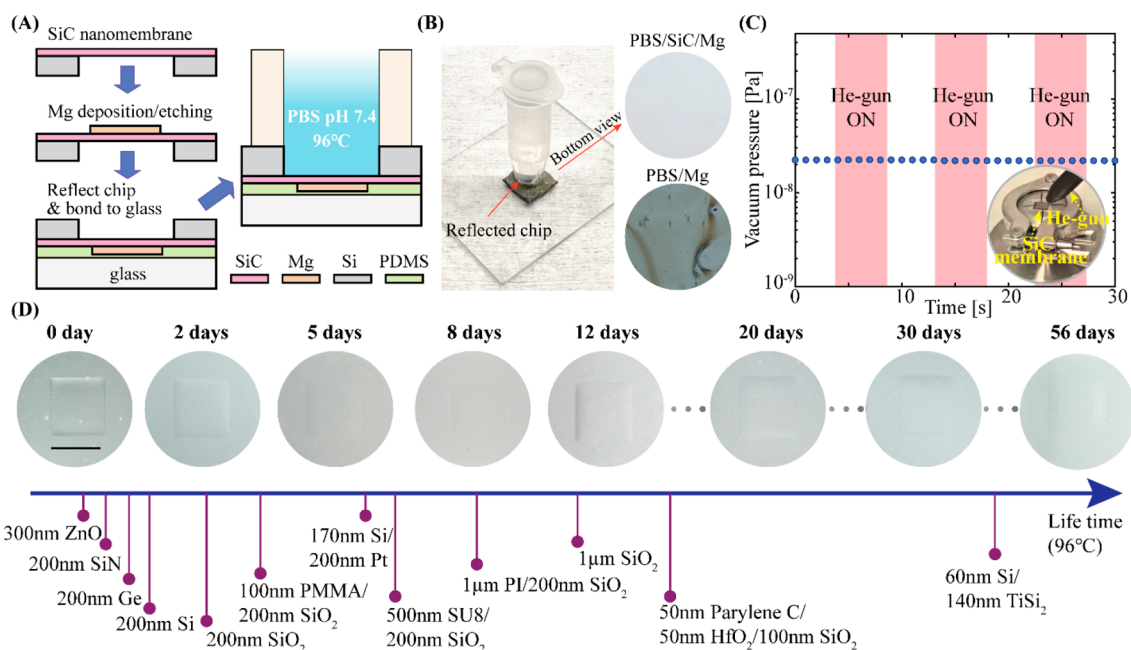


Figure 3. Water barrier test of 230 nm SiC nanomembranes. (A) Fabrication of the test chips. (B) Photograph of a testing device with a Teflon reservoir to contain PBS at pH 7.4 and 96 °C. (C) Helium leak test on free-standing SiC nanomembranes, confirming the absence of pinholes. (D) Evaluation of water barrier properties of SiC nanomembranes in PBS at 96 °C, in comparison to the lifetimes of other materials with similar or larger thickness.

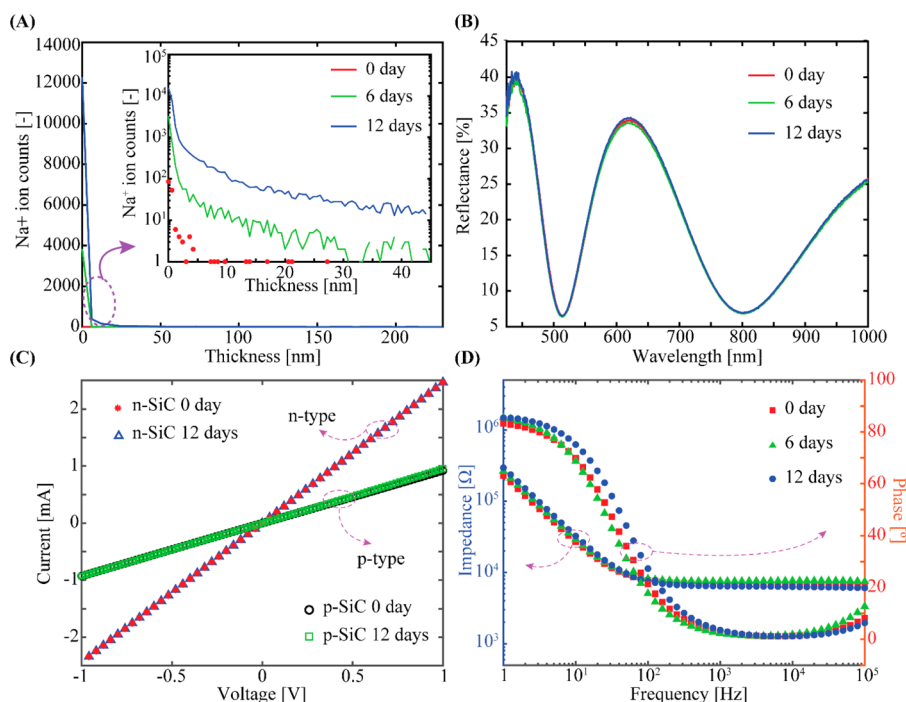


Figure 4. Ion barrier tests of 230 nm SiC nanomembranes. (A) Secondary ion mass spectroscopy measurement of Na^+ diffusion into SiC nanomembranes after soaking in $1\times$ PBS at 96 °C for 0, 6, and 12 days with a Na^+ concentration of 0.14 M. (B) Ellipsometry measurements of the soaked films showing excellent stability of their optical properties. (C) Electrical properties of a normally doped film ($N_d = 10^{18} \text{ cm}^{-3}$ for p-type and $N_d = 5 \times 10^{19} \text{ cm}^{-3}$ for n-type), indicating stability in its electrical properties. (D) Data showing the invariance of EIS in SiC electrodes in fluidic environments.

due to the negligible rate of hydrolysis for SiC, as shown in Figure 2. The possibility of pinholes in our SiC nanomembranes was examined using a helium leak test in which the SiC nanomembranes were mounted on a vacuum chamber, and helium gas was purged through the membrane using a high-pressure gun. Helium was utilized as the detecting gas due to its

small atomic volume (with a radius of 0.05 nm). The experimental result indicated negligible pressure change under purging/depurging with helium, indicating that the SiC nanomembranes are free of pinholes. Figure 3D shows optical images of Mg films after the 230 nm SiC nanomembranes were soaked in PBS at 96 °C, clearly illustrating the presence of

unperturbed Mg after 60 days. As a means of comparison, we plotted the time scale of other semiconductors (e.g., Si, Ge, and ZnO),^{9,10,44} insulators (e.g., SiO₂, SiN_x),^{12,14} as well as multilayer stacks (e.g., SiO₂/HfO₂, PI/SiO₂, parylene/HfO₂/SiO₂)⁴⁵ published previously (Figure 3C, bottom). The results demonstrate that SiC nanomembranes offer excellent barrier properties.

Another key characteristic for long-term implantation is in the prevention of ion diffusion. Many different types of ions exist in biofluidic media, perhaps most notably Na⁺ and K⁺. The diffusion of ions can change the electrical properties of the functional materials as well as the dielectric constant of the encapsulation layer, thereby destabilizing the performance of biointegrated devices. Ion diffusion is a critical problem for SiO₂, where intrinsic penetration through the material itself leads to drifts in the threshold voltages of underlying transistors, for example.^{12,14} For the case of SiN_x, the presence of pinholes leads to ion penetration. We utilized 1× PBS, pH 7.4, which contains 137 mM Na⁺ ions to explore the Na⁺ ion diffusion rate into SiC nanomembranes. Three sets of SiC/Si samples with dimensions of 10 mm × 10 mm were immersed in 1× PBS at 96 °C for 0, 6, and 12 days. The relative concentrations of the Na⁺ ions in the SiC films were then measured using secondary ion mass spectrometry (SIMS), where a Au beam was utilized to remove the material and an O₂ beam was employed to detect the Na⁺ ions. Figure 4A shows the Na⁺ depth profile in these films. The results show that the ion concentration increases with increasing soaking period, consistent with X-ray photoelectron spectroscopy (XPS) measurements (Figure S3). The ion distribution sharply decreased by 3 orders of magnitude from a depth of 50 nm and reached the detection limit of the SIMS measurement at a depth of 100 nm for the 12 day samples, implying an extremely low ion diffusivity through the SiC films. Therefore, crystalline SiC nanomembranes can serve as an excellent ion barrier to protect other electronic components embedded underneath. The change in ellipsometry spectra provides further insights into the extent of ion diffusion. Figure 4(B) shows a consistent optical reflectance of 230 nm SiC films after immersion in PBS at 96 °C for 0, 6, and 12 days. This result demonstrates the superiority of SiC over thermal oxide, which exhibits a significant blue shift of 200 nm wavelength in its optical reflectance spectra after only 14 h of soaking in PBS at 96 °C (film thickness of thermal oxide = 320 nm).¹⁴ The current–voltage (*I*–*V*) characteristics further confirm the negligible influence of diffused ions on the electrical conductance of both p-type (carrier concentration = 5 × 10¹⁸ cm⁻³, hole mobility = 30 cm² V⁻¹ s⁻¹) and n-type (carrier concentration = 5 × 10¹⁹ cm⁻³, electron mobility = 100 cm² V⁻¹ s⁻¹) SiC films (Figure 4C). The SiC films also show consistent electrochemical impedance spectra (EIS) (with a small difference in impedance and phase falling within the variation between samples fabricated from the same wafer, Figure S6), which indicates its potential as an excellent, long-term Faradaic interface (Figure 4D). The impedance of highly doped SiC electrodes (with a surface area of 200 μm × 200 μm and a thickness of 230 nm) at 1 kHz was approximately 10 kΩ, which is in the same range as highly doped 4H-SiC and 3C-SiC shank electrodes reported in the literature.^{38,39} This value is well below 600 kΩ, indicating its suitability for electrophysiological recording applications.⁴⁶

For implantable electronics, the biocompatibility of the functional materials plays a crucial role to avoid the risk of rejection. A common way to test the biocompatibility of a material is through *in vitro* cell cultures. We employed mouse

fibroblast (MF) cells (e.g., for animal model study) and human dermal fibroblast (HDF) cell lines (e.g., for practical health care applications) as indicators of SiC biocompatibility. Prior to cell culture, the SiC nanomembranes were cleaned with 80% ethanol followed by surface UV exposure for 30 min. The cells were seeded on the surface of SiC followed by storing at 37 °C for 3 days. The high optical transmittance of the free-standing SiC nanomembranes in the visible range enables cell morphology observation and imaging using inverted fluorescent microscopes (Figure 5A). Figure 5B–E shows bright-field and fluorescent microscopy images of HDF cells after 24 h. The increase in the number of cells after 24 h indicates a good proliferation in the HDF cells (Figure 5B). The formation of functional actin fibers and cell nucleic (stained with DAPI) clearly captures the extensive stress of the HDF cytoskeleton, confirming that the cells well anchored on the SiC surface. The proper distribution of mitochondria throughout all cells strongly implies their healthiness and regular growth. Good proliferation was also observed in MF cells with clear formation of cytoskeleton and nucleic structures (Figure 5F). Figure 5G shows the quantified viability of the HDF and MF cells after being cultured on SiC nanomembranes for 72 h, which is comparable to that of control samples (Figures S7 and S8). Employing a similar cell culture protocol, we also observed good cell proliferation in low-doped SiC (Figure S9), indicating that varying the doping concentration does not affect the biocompatibility of SiC nanomembranes.

The above experimental results clearly highlight the potential of SiC nanomembranes for long-lived bioimplantable applications as the material shows a zero hydrolysis rate, negligible water penetration, extremely low ion diffusivity, and good cell level biocompatibility. However, SiC-on-Si is a rigid platform that is not suitable for soft tissue interfaces. To overcome this mechanical mismatch, we developed a transfer technique to form flexible crystalline SiC electronics, as illustrated in Figure 6A. Free-standing SiC nanomembranes with dimensions varying from a few hundred micrometers up to several millimeters were formed by use of KOH etching to remove the silicon underneath. The mechanical robustness was investigated using a burst test, showing that membranes with a window size of 1 mm × 1 mm can hold a pressure of up to 1.5 bar (Figure S10). This mechanical strength allows for photoresist, spin-coating, and wet-etching in liquid media, including the ability to execute complete processes on free-standing SiC nanomembranes to yield microstructures with a large aspect ratio (e.g., thickness/length ~ 1:10⁴). Figure 6B demonstrates a direct photolithography sequence that involves aluminum (Al) hard masks patterned on the free-standing areas of nanomembranes. Etching the SiC through this mask using inductive coupling plasma (SF₆ + O₂) followed by removal of the Al resulted in free-standing SiC microstructures such as microbridges and microtrampolines (Figure S11). We note that anisotropic etching of the Si (through the back SiC hard mask) created SiC microtrenches (aligned along [110] crystallographic orientation) to connect all devices as a part of a full 6 in. SiC/Si wafer. By clipping these trenches, each SiC nanomembrane on silicon chips can easily be separated, enabling either selective transfer (e.g., a single device at a time) or a large collection of SiC devices (e.g., an array of nanomembranes) for particular applications (Figure 6B, left). The free-standing SiC structures can be stamped onto a polydimethylsiloxane (PDMS) slab. By utilizing strain concentration designs, the stamped SiC structures can be detached from the Si substrates at the anchor

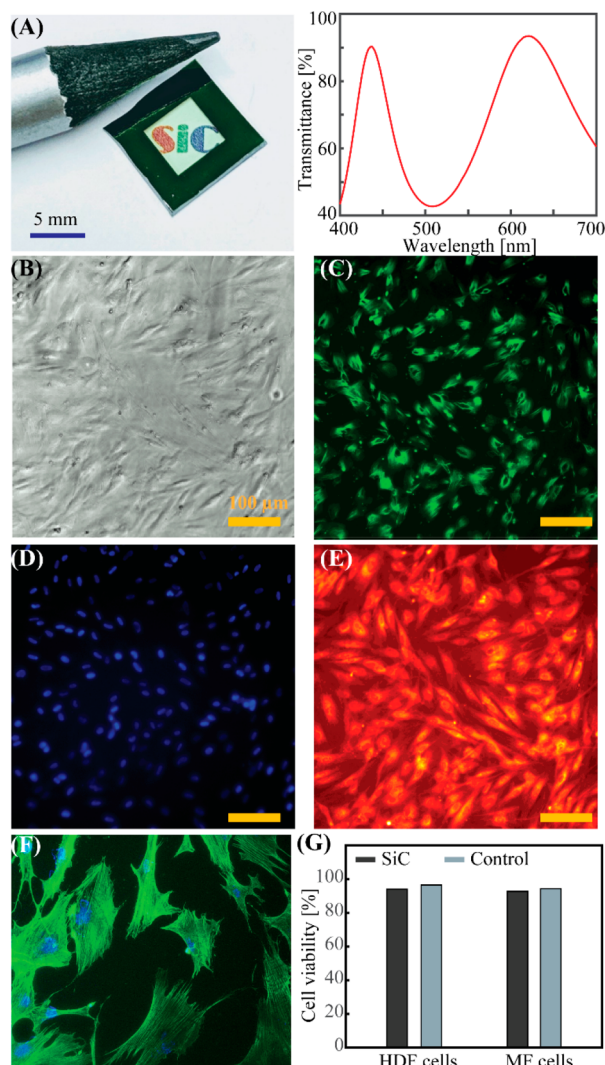


Figure 5. Biocompatibility of SiC nanomembranes tested with mouse (for animal model studies) and human (for practical health care applications) cells. (A) Optical transmittance of 230 nm thick SiC nanomembranes. (B) Bright-field images indicate cell adherence. (C) Cells show functional actin fiber formation. (D) All cells were counterstained for nuclei using DAPI (blue). (E) Mitochondria distribution throughout the cell was detected by using mitochondria-specific dye MitoTracker Deep Red. (F) Fluorescence from MF cells stained with actin and DAPI. (G) Trypan blue (TB) exclusion test shows no significant difference in percentage of viable cells.

parts due to fracture that follows application of small pressures using the PDMS slab (Figure S12). The detached SiC nanomembranes can then be stamped onto a polyimide layer spin-coated on a Kapton film/PDMS/glass substrate. Due to the larger adhesion strength between the SiC and polyimide in comparison to the SiC and PDMS, the SiC nanomembranes remained on the polyimide (PI) film upon removal of the PDMS slab. Subsequently, a photoresist was spin-coated and patterned followed by metal deposition and lift-off, forming metal contacts for SiC devices. Spin-coating another PI capping layer followed by opening windows (using O_2 plasma) for the SiC can further improve the adhesion between SiC and the PI substrate (Figure 6D). Finally, peeling off the metal/SiC/PI from the PDMS/glass substrate forms a flexible SiC-on-PI platform that can establish conformal contacts with curved surfaces (Figure 6E). The above

fabrication technology is applicable to a wide range of epitaxial material systems (e.g., III-Nitride on Si, or diamond-like carbon film on Si) where there is no sacrificial layer sandwiched between functional films and the handling substrate, as in the case of silicon-on-insulator wafers.

We estimated the bendability of the transferred SiC nanomembranes using the conventional plate and shell model: $M = E_{SiC}t_{SiC}^3/12$, where E_{SiC} and t_{SiC} are the Young's modulus and the thickness of the SiC nanomembranes, respectively. This scaling suggests that decreasing the thickness of the SiC from bulk dimensions (e.g., 300 μm) to nanomembranes (e.g., 10 nm) will reduce the bending stiffness by 14 orders of magnitude (Figure 7A, solid line). In addition, with the same dimensions, Si nanomembranes are approximately 2 times more flexible than SiC nanomembranes owing to differences in the Young's moduli. As implantable electronics consist of not only the functional layer (i.e., SiC, or Si nanomembranes) but also the supporting soft substrate (i.e., PI), a bilayer model is needed to determine the bending stiffness of the SiC-on-PI platform:⁴⁷

$$M_{SiC/PI} = \frac{E_{SiC}^2 t_{SiC}^4 + E_{PI}^2 t_{PI}^4 + E_{SiC} E_{PI} t_1 t_2 (2t_{SiC}^2 + 3t_{SiC} t_{PI} + 2t_{PI}^2)}{12(E_{SiC} t_{SiC} + E_{PI} t_{PI})}$$

where E and t are the Young's modulus and thickness of each layer, respectively. The results show that by transferring SiC onto PI, the bending stiffness is reduced by 1 million times compared to that of the bulk SiC material (Figure 7A, dashed lines). Furthermore, the bending stiffness of the bilayer is dominated by the PI layer (with its thickness being fixed at 14 μm) when the thickness of the nanomembranes reaches below ~ 300 nm for both SiC and Si (i.e., $M_{SiC/PI} \approx M_{Si/PI}$). The flexibility of the transferred SiC films was experimentally demonstrated using a buckling setup in which a bending radius of 6 mm (corresponding to a strain of $\epsilon = [t/2]/R \approx 0.12\%$) was applied using a cyclic linear actuator (Figure 7B). The stability in the measured electrical resistance of the SiC over 1000 bending cycles confirms the robust bendability of the SiC/PI platform (Figure 7C). The as-transferred SiC resistors (with Au/Cr electrodes) were also soaked in PBS at 96 $^\circ\text{C}$ for several days as a long-term operational test. The results show a consistent electrical conductivity for SiC-on-PI, over a period of at least 18 days in PBS, pH 7.4, at 96 $^\circ\text{C}$. Using thermal oxide as a reference material (lifetime $\propto \exp(E_a/k_B T)$), the operating time scale of SiC/PI without any encapsulating layer is estimated to be over 100 years at human body temperature. The findings demonstrate that although SiC-on-PI offers a comparable mechanical flexibility as Si-on-PI, it also provides clear advantages regarding corrosive tolerance and long-term stability.

An attractive feature of SiC over metals is in the capacity to engineer the electrical properties (e.g., through doping impurities) for sensing applications. We demonstrated this point by constructing multifunctional SiC devices for measuring different biophysical parameters. We developed SiC temperature sensors using low-doped SiC films ($N_d = 10^{16}$ to 10^{17} cm^{-3}) transferred onto PI following the above fabrication process. The low-doped films were utilized because, generally, they offer a temperature sensitivity higher than that of highly doped samples.⁴⁸ The temperature sensing mechanism is based on the thermoresistive effect in the SiC,⁴⁹ where the electrical conductance of SiC increases with increasing temperatures due to the thermal activation of charge carriers: $\sigma \propto \exp(-E_a/k_B T)$ (Figure 7E). Figure 7F plots the temperature resistance of

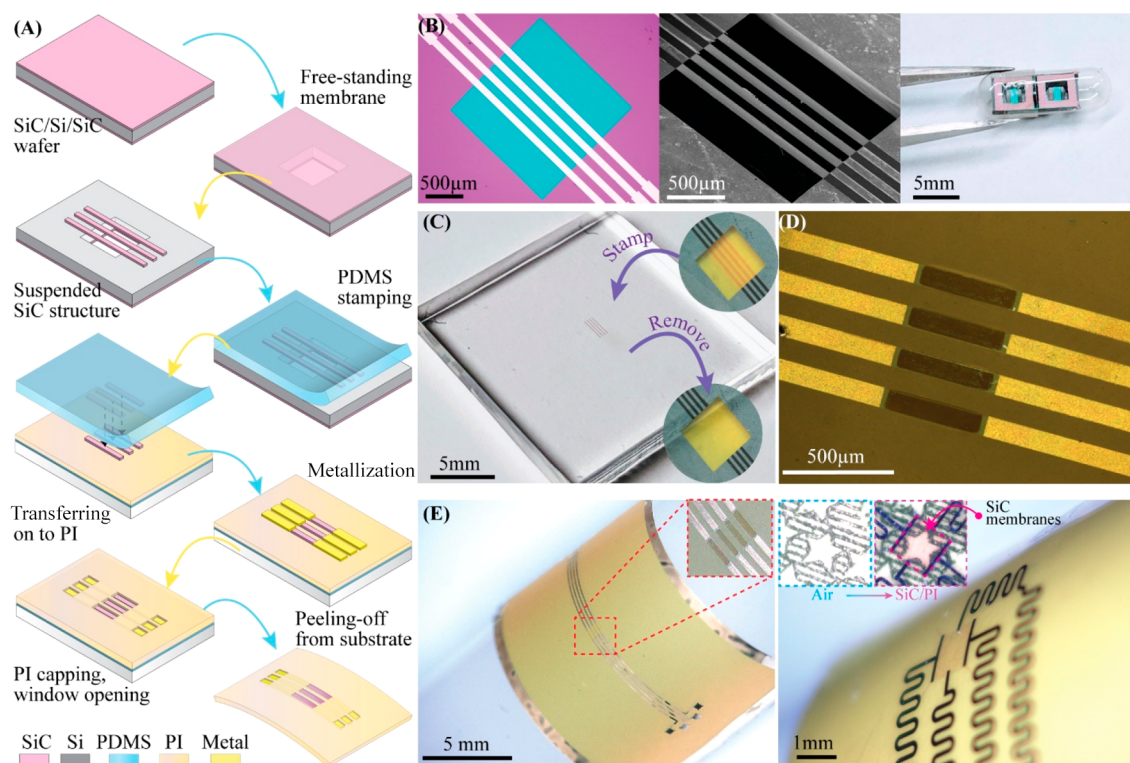


Figure 6. Transferring SiC onto PI using a transfer printing process using PDMS slabs. Fabrication flow for the transfer. (B) Photograph of SiC free-standing structures. Left: Photolithography on free-standing SiC nanomembranes. Middle: Suspended SiC microbridges. Right: Free-standing SiC chips were clipped into small devices and stored in gelatin capsule for selective transferring. Photograph of SiC nanomembranes stamped on a PDMS slab (inset SiC/Si chip before and after stamping). (D) SiC transferred on a PI/glass substrate. (E) Flexible SiC-on-PI devices wrapped around a curved surface (diameter = 12 mm).

coefficient ($TCR = (\Delta R/R)\Delta T$) in a temperature range of 25 to 80 °C. The results show a high TCR in SiC of approximately $-12\,000$ ppm/K at 37 °C, which is 3.5 times larger than that of gold (3400 ppm/K). This large TCR of low-doped SiC along with its stability in biofluids allows continuous and long-lived temperature recording.

Besides the thermoresistive effect, SiC materials also possess a significant piezoresistive phenomenon that follows from modulation of the band gap of SiC under a mechanical load.^{44,47} We demonstrated SiC/PI strain sensors by peeling off the SiC/PI from the glass substrate and attaching it onto an acrylic cantilever (Figure 7G). Mechanical strains were then applied to the SiC sensors by deflecting the free tip of the cantilever (Figure S14). Figure 7H shows the response of the sensors to external forces, indicating that the electrical conductance of p-type SiC decreases with increasing the applied tensile force from 0 to 392 mN. The sensors also exhibit good repeatability over 40 bending cycles (Figure 7H, bottom). To estimate the actual strain induced in the SiC sensors, we employed a metal strain gauge adhered on a similar acrylic cantilever. Figure 7I shows the relative resistance change of the SiC sensors in comparison to that of the commercial strain gauge, indicating a good linearity and a higher sensitivity in the as-transferred SiC devices. The gauge factor ($GF = [\Delta R/R]/\epsilon$) of the SiC was found to be 27.4, which is approximately 14 times higher than that of metals. This significant piezoresistive effect in flexible SiC suggests great potential for the development of long-lived mechano-physiological recording systems for monitoring processes such as bladder expansion, lung respiration, and heart contractions.

CONCLUSION

The findings in this work demonstrate that flexible platforms based on nanomembranes of SiC offer many attractive features as long-lived implantable devices owing to its chemical stability in biofluids, outstanding water barrier characteristics, and extremely low permeability to ions, suitable for stable operation with projected lifetimes of many decades in biological environments. The fabrication approach to release and transfer nanomembrane SiC onto flexible polymer substrates such as PI establishes a route to systems well-suited for integration with soft tissues, enabling the development of unusual wide band gap semiconducting devices with bendable, foldable, and flexible formats and advanced functional modes. The robustness of the SiC biointerface along with its interesting physical properties, including thermoresistive and piezoresistive effects, suggests a promising path toward advanced versions of long-term implantable electronics for chronic neural and cardiac electrophysiology.

METHOD

SiC Film Deposition. The SiC films were deposited onto a Si substrate using a hot wall chamber (Epiflex) at a temperature of 1250 °C. Prior to thin film deposition, the Si substrate was cleaned using the standard process RCA (Radio Corporation of America). The growth process started with carbonization of the Si surface followed by an alternating supply of epitaxy cycles where SiH_4 and C_2H_6 were utilized as Si and C precursors. To form n-type and p-type SiC, an *in situ* doping method was employed in which NH_3 and TMAI were the dopants for n-type and p-type, respectively.

Device Development. *Fabrication of Free-Standing SiC Structures.* The backside SiC layer was used as a hard mask to form

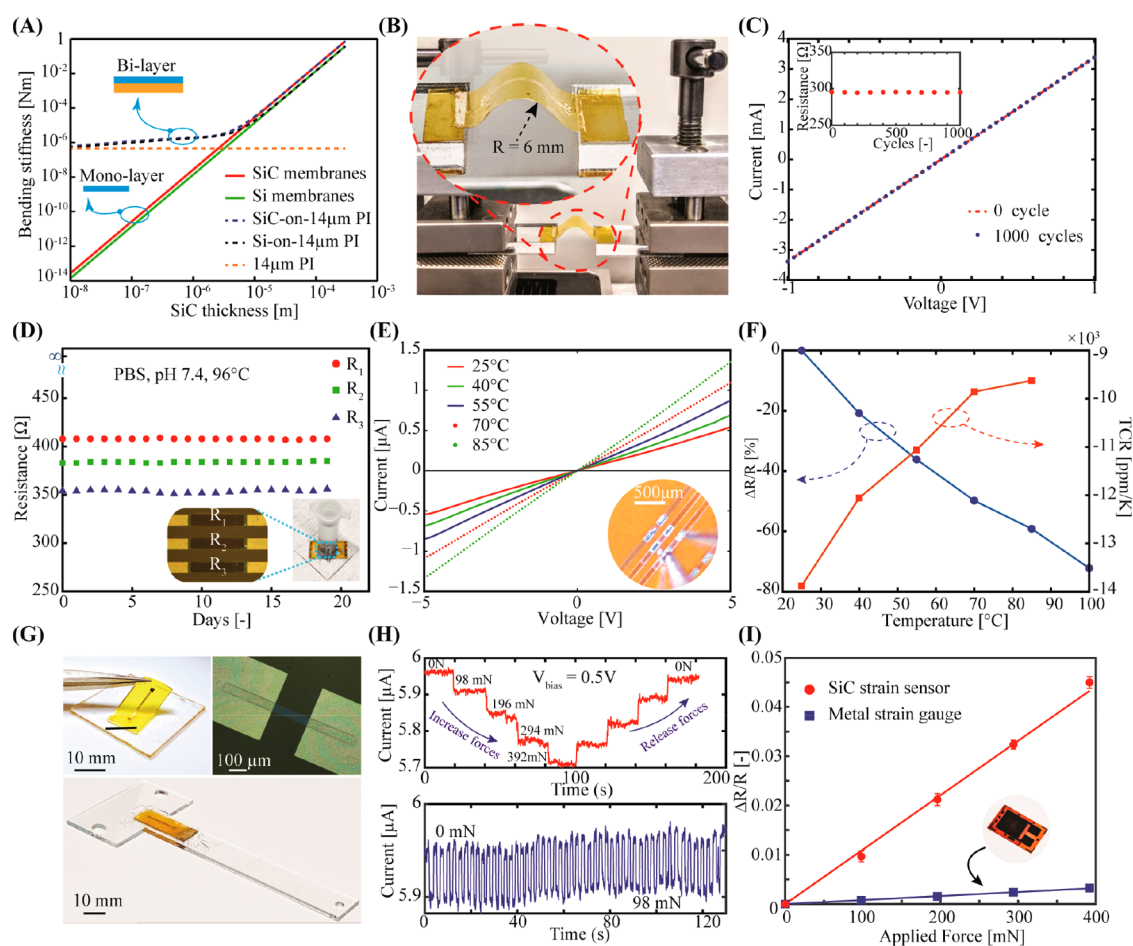


Figure 7. Demonstration of multifunctionality in the SiC/PI platform. (A) Computed estimation of the bendability of SiC/PI. (B,C) Experimental setup and electrical conductivity of SiC/PI upon several bending cycles. (D) Demonstration of long-lived SiC/PI devices subjected to PBS at 96 °C. (E,F) SiC/PI temperature sensors with a relatively large TCR. (G) Photograph of flexible SiC strain sensors peeled from the glass substrate. (H,I) Response of the sensors to tensile strains and the linear relationship between resistance change and applied strain.

free-standing SiC membranes on the top surface. The AZ5214 photoresist was spin-coated and patterned to form microscale window structures on the SiC bottom layers. This SiC bottom layer was then dry-etched using inductively coupled plasma etching ($\text{SF}_6 + \text{O}_2$) for about 2 min to expose the silicon layer. The exposed Si area was then wet-etched using KOH (30%) at 80 °C for 10 h, leaving square-shaped free-standing SiC nanomembranes (Figure 1D). The wafer was then cleaned using RCA to remove Si contamination. Next, 100 nm aluminum was deposited on the free-standing SiC films to form a hard mask for subsequent SiC plasma etching. The AZ5214 photoresist was spin-coated on Al/Si and patterned on free-standing membranes to form various microstructures including microbeams and trampolines. The exposed SiC areas were then plasma-etched, leaving free-standing Al/SiC structures. The Al mask was completely removed using wet-etching to form free-standing SiC structures for subsequent transfer using PDMS slabs. Further details are available in the Supporting Information, Figure S1.

Fabrication of Hydrolysis Testing Samples. Photoresist AZ5214 was spin-coated and developed to form microwindows on testing materials. A 100 nm thick Ti film was sputtered and then lifted-off, leaving opening areas of p^{++} Si, thermal oxide, and SiC. Next, these samples were diced into 4 mm \times 4 mm chips and inserted into a PBS-containing Teflon bottle at 96 °C.

Fabrication of Water Diffusion Testing Samples. Photoresist AZ5214 was spin-coated and developed on free-standing SiC membranes. Ti/Mg (10 nm/150 nm) was sputtered and etched, leaving square structures well aligned with the SiC windows.

Subsequently, a thin layer of PDMS was spin-coated at 4000 rpm on a glass slide to form an adhesion layer. Next, the Mg/SiC chip was flipped and embedded onto the wet PDMS/glass slide and then heated to 150 °C for 5 min to fix the SiC chip on the glass slide. Finally, a Teflon reservoir was attached on the bottom side of the chip using high-temperature epoxy to contain the PBS solution. The transparency of glass and PDMS enables direct observation of the Mg film during the wafer diffusion experiment (Figure S2).

Electrical Measurement. The current–voltage (I – V) characteristics of all samples were measured using a semiconductor device parameter analyzer (Agilent B1500). The temperature sensors were tested using a thermal chuck where electrical contact was formed using a probe station. The strain sensors were characterized using the current–time (I – t) mode, in which the bias voltage applied to the sensors was fixed at 0.5 V and the change in the output current under the applied force was continuously recorded.

ASSOCIATED CONTENT

Supporting Information

The Supporting Information is available free of charge on the ACS Publications website at DOI: 10.1021/acsnano.9b05168.

Step-by-step fabrication process, characterization methodologies, and details of the cell culture protocol, as well as figures including the hydrolysis rate, chemical inertness, and bio compatibility of low-doped SiC membranes, and photographs of transferred SiC nanomembranes (PDF)

AUTHOR INFORMATION

Corresponding Authors

*E-mail: h.phan@griffith.edu.au.

*E-mail: jrogers@northwestern.edu.

*E-mail: nam-trung.nguyen@griffith.edu.au.

ORCID 

Hoang-Phuong Phan: 0000-0002-1724-5667

Toan Dinh: 0000-0002-7489-9640

Enming Song: 0000-0002-2658-904X

Muhammad J.A. Shiddiky: 0000-0003-4526-4109

Dzung Dao: 0000-0002-6348-0879

Yusuke Yamauchi: 0000-0001-7854-927X

Notes

The authors declare no competing financial interest.

ACKNOWLEDGMENTS

This work was partially funded by the linkage Grants LP150100153 and LP160101553 from the Australian Research Council (ARC). The 3C-SiC material was developed and supplied by Leonie Hold and Alan Iacopi of the Queensland Microtechnology Facility, part of the Queensland node—Griffith—of the Australian National Fabrication Facility, a company established under the National collaborative Research Infrastructure Strategy to provide nano and microfabrication facilities for Australia's researchers. The authors acknowledge support from the Center for Bio-Integrated Electronics at Northwestern University. H.P.P. acknowledges research grants from Griffith University Postdoctoral Fellowship (GUPF) and the Griffith University's New Researcher Grants (GUNRG).

REFERENCES

- (1) Jeong, J.-W.; McCall, J. G.; Shin, G.; Zhang, Y.; Al-Hasani, R.; Kim, M.; Li, S.; Sim, J. Y.; Jang, K. I.; Shi, Y.; Hong, D. Y.; Liu, Y.; Schmitz, G. P.; Xia, L.; He, Z.; Gamble, P.; Ray, W. Z.; Huang, Y.; Bruchas, M. R.; Rogers, J. A. Wireless Optofluidic Systems for Programmable *In Vivo* Pharmacology and Optogenetics. *Cell* **2015**, *162*, 662–674.
- (2) Dai, X.; Zhou, W.; Gao, T.; Liu, J.; Lieber, C. M. Three-Dimensional Mapping and Regulation of Action Potential Propagation in Nanoelectronics Innervated Tissues. *Nat. Nanotechnol.* **2016**, *11*, 776–782.
- (3) Jun, J. J.; Steinmetz, N. A.; Siegle, J. H.; Denman, D. J.; Bauza, M.; Barbarits, B.; Lee, A. K.; Anastassiou, C. A.; Andrei, A.; Aydın, C.; Barbic, M.; Blanche, T. J.; Bonin, V.; Couto, J.; Dutta, B.; Gratiy, S. L.; Gutnisky, D. A.; Häusser, M.; Karsh, B.; Ledochowitsch, P.; et al. Fully Integrated Silicon Probes for High-Density Recording of Neural Activity. *Nature* **2017**, *551*, 232–236.
- (4) Formento, E.; Minassian, K.; Wagner, F.; Mignardot, J. B.; Le Goff-Mignardot, C. G.; Rowald, A.; Bloch, J.; Micera, S.; Capogrosso, M.; Courtine, G. Electrical Spinal Cord Stimulation Must Preserve Proprioception to Enable Locomotion in Humans with Spinal Cord Injury. *Nat. Neurosci.* **2018**, *21*, 1728–1741.
- (5) Someya, T.; Bao, Z.; Malliaras, G. G. The Rise of Plastic Bioelectronics. *Nature* **2016**, *540*, 379–385.
- (6) Viventi, J.; Kim, D.-H.; Moss, J. D.; Kim, Y.-S.; Blanco, J. A.; Annetta, N.; Hicks, A.; Xiao, J. L.; Huang, Y.; Callans, D. J.; Rogers, J. A.; Litt, B. A. Conformal Bio-Interfaced Class of Silicon Electronics for Mapping Cardiac Electrophysiology. *Sci. Transl. Med.* **2010**, *2*, 24ra22.
- (7) Mickle, A. D.; Won, S. M.; Noh, K. N.; Yoon, J.; Meacham, K. W.; Xue, Y.; McIlvried, L. A.; Copits, B. A.; Samineni, V. K.; Crawford, K. E.; Kim, D. H.; Srivastava, P.; Kim, B. H.; Min, S.; Shiu, Y.; Yun, Y.; Payne, M. A.; Zhang, J.; Jang, H.; Li, Y.; et al. A Wireless Closed-Loop System for Optogenetic Peripheral Neuromodulation. *Nature* **2019**, *565*, 361–365.

(8) Rotenberg, M. Y.; Tian, B. Bioelectronic Devices Long-Lived Recordings. *Nat. Biomed. Eng.* **2017**, *1* (3), 0048.

(9) Hwang, S. W.; Park, G.; Edwards, C.; Corbin, E. A.; Kang, S. K.; Cheng, H.; Song, J. K.; Kim, J. H.; Yu, S.; Ng, J.; Lee, J. E.; Kim, J.; Yee, C.; Bhaduri, B.; Su, Y.; Omennetto, F. G.; Huang, Y.; Bashir, R.; Goddard, L.; Popescu, G.; et al. Dissolution Chemistry and Biocompatibility of Single-Crystalline Silicon Nanomembranes and Associated Materials for Transient Electronics. *ACS Nano* **2014**, *8*, 5843–5851.

(10) Kang, S. K.; Park, G.; Kim, K.; Hwang, S. W.; Cheng, H.; Shin, J.; Chung, S.; Kim, M.; Yin, L.; Lee, J. C.; Lee, K. M.; Rogers, J. A. Dissolution Chemistry and Biocompatibility of Silicon-and Germanium-based Semiconductors for Transient Electronics. *ACS Appl. Mater. Interfaces* **2015**, *7*, 9297–9305.

(11) Chang, J. K.; Chang, H. P.; Guo, Q.; Koo, J.; Wu, C. I.; Rogers, J. A. Biodegradable Electronic Systems in 3D, Heterogeneously Integrated Formats. *Adv. Mater.* **2018**, *30*, 1704955.

(12) Fang, H.; Zhao, J.; Yu, K. J.; Song, E.; Farimani, A. B.; Chiang, C. H.; Jin, X.; Xue, Y.; Xu, D.; Du, W.; Seo, K. J.; Zhong, Y.; Yang, Z.; Won, S. M.; Fang, G.; Choi, S. W.; Chaudhuri, S.; Huang, Y.; Alam, M. A.; Viventi, J.; et al. Ultrathin, Transferred Layers of Thermally Grown Silicon Dioxide as Biofluid Barriers for Biointegrated Flexible Electronic Systems. *Proc. Natl. Acad. Sci. U. S. A.* **2016**, *113*, 11682–11687.

(13) Song, E.; Lee, Y. K.; Li, R.; Li, J.; Jin, X.; Yu, K. J.; Xie, Z.; Fang, H.; Zhong, Y.; Du, H.; Zhang, J.; Fang, G.; Kim, Y.; Yoon, Y.; Alam, M. A.; Mei, Y.; Huang, Y.; Rogers, J. A. Transferred, Ultrathin Oxide Bilayers as Biofluid Barriers for Flexible Electronic Implants. *Adv. Funct. Mater.* **2018**, *28*, 1702284.

(14) Song, E.; Fang, H.; Jin, X.; Zhao, J.; Jiang, C.; Yu, K. J.; Zhong, Y.; Xu, D.; Li, J.; Fang, G.; Du, H.; Zhang, Y.; Park, J. M.; Huang, Y.; Alam, M. A.; Mei, Y.; Rogers, J. A. Thin, Transferred Layers of Silicon Dioxide and Silicon Nitride as Water and Ion Barriers for Implantable Flexible Electronic Systems. *Adv. Elec. Mater.* **2017**, *3*, 1700077.

(15) de Beeck, M. O.; Jarboui, A.; Cauwe, M.; Declercq, H.; Uytterhoeven, G.; Cornelissen, M.; Vanfleteren, J.; Van Hoof, C. Improved Chip & Component Encapsulation by Dedicated Diffusion Barriers to Reduce Corrosion Sensitivity in Biological and Humid Environments. *IEEE European Microelectronics Packaging Conference*, September 2013; pp 1–6.

(16) Lee, Y. K.; Yu, K. J.; Kim, Y.; Yoon, Y.; Xie, Z.; Song, E.; Luan, H.; Feng, X.; Huang, Y.; Rogers, J. A. Kinetics and Chemistry of Hydrolysis of Ultrathin, Thermally Grown Layers of Silicon Oxide as Biofluid Barriers in Flexible Electronic Systems. *ACS Appl. Mater. Interfaces* **2017**, *9*, 42633–42638.

(17) Li, J.; Song, E.; Chiang, C. H.; Yu, K. J.; Koo, J.; Du, H.; Zhong, Y.; Hill, M.; Wang, C.; Zhang, J.; Chen, Y.; Tian, L.; Zhong, Y.; Fang, G.; Viventi, J.; Rogers, J. A. Conductively Coupled Flexible Silicon Electronic Systems for Chronic Neural Electrophysiology. *Proc. Natl. Acad. Sci. U. S. A.* **2018**, *115*, E9542–E9549.

(18) Li, J.; Li, R.; Du, H.; Zhong, Y.; Chen, Y.; Nan, K.; Won, S. M.; Zhang, J.; Huang, Y.; Rogers, J. A. Ultrathin, Transferred Layers of Metal Silicide as Faradaic Electrical Interfaces and Biofluid Barriers for Flexible Bioelectronic Implants. *ACS Nano* **2019**, *13*, 660–670.

(19) Jiang, Y.; Li, X.; Liu, B.; Yi, J.; Fang, Y.; Shi, F.; Gao, X.; Sudzilovsky, E.; Parameswaran, R.; Koehler, K.; Nair, V.; Yue, J.; Guo, K. H.; Fang, Y.; Tsai, H. M.; Freyermuth, G.; Wong, R. C. S.; Kao, C. M.; Chen, C. T.; Nicholls, A. W.; et al. Rational Design of Silicon Structures for Optically Controlled Multiscale Biointerfaces. *Nat. Biomed. Eng.* **2018**, *2*, 508–521.

(20) Park, S.; Frank, J. A.; Anikeeva, P. Silicon Biointerfaces for all Scales. *Nat. Bio. Eng.* **2018**, *2*, 471–472.

(21) Feiner, R.; Dvir, T. Tissue–Electronics Interfaces: from Implantable Devices to Engineered Tissues. *Nat. Rev. Mater.* **2018**, *3*, 17076.

(22) Sun, W.; Puzas, J. E.; Sheu, T. J.; Liu, X.; Fauchet, P. M. Nano-to Microscale Porous Silicon as a Cell Interface for Bone-Tissue Engineering. *Adv. Mater.* **2007**, *19*, 921–924.

- (23) Lee, T. H.; Bhunia, S.; Mehregany, M. Electromechanical Computing at 500°C with Silicon Carbide. *Science* **2010**, *329*, 1316–1318.
- (24) Nguyen, T. K.; Phan, H. P.; Dinh, T.; Han, J.; Dimitrijević, S.; Tanner, P.; Faisal, A. R. M.; Zhu, Y.; Nguyen, N. T.; Dao, D. V. Experimental Investigation of Piezoresistive Effect In *p*-Type 4H–SiC. *IEEE Electron Device Lett.* **2017**, *38*, 955–958.
- (25) Nguyen, T. K.; Phan, H. P.; Dinh, T.; Faisal, A. R. M.; Nguyen, N. T.; Dao, D. V. High-Temperature Tolerance of the Piezoresistive Effect in *p*-4H–SiC for Harsh Environment Sensing. *J. Mater. Chem. C* **2018**, *6*, 8613–8617.
- (26) Phan, H. P.; Dinh, T.; Kozeki, T.; Qamar, A.; Namazu, T.; Dimitrijević, S.; Nguyen, N. T.; Dao, D. V. Piezoresistive Effect in *p*-Type 3C–SiC at High Temperatures Characterized Using Joule Heating. *Sci. Rep.* **2016**, *6*, 28499.
- (27) Lantz, M. A.; Gotsmann, B.; Jaroenapibal, P.; Jacobs, T. D.; O'Connor, S. D.; Sridharan, K.; Carpick, R. W. Wear-Resistant Nanoscale Silicon Carbide Tips for Scanning Probe Applications. *Adv. Funct. Mater.* **2012**, *22*, 1639–1645.
- (28) Phan, H. P.; Nguyen, T. K.; Dinh, T.; Qamar, A.; Iacopi, A.; Lu, J.; Dao, D. V.; Rais-Zadeh, M.; Nguyen, N. T. Wireless Battery-Free SiC Sensors Operating in Harsh Environments Using Resonant Inductive Coupling. *IEEE Electron Device Lett.* **2019**, *40*, 609–612.
- (29) Hong, Z.; Cheng, L.; Zhang, L.; Wang, Y. Internal Friction Behavior of C/SiC Composites with Environmental Barrier Coatings in Corrosive Environment. *Int. J. Appl. Ceram. Technol.* **2011**, *8*, 342–350.
- (30) Cutroneo, M.; Musumeci, P.; Zimbone, M.; Torrisi, L.; La Via, F.; Margarone, D.; Velyhan, A.; Ullschmied, J.; Calcagno, L. High Performance SiC Detectors for MeV Ion Beams Generated by Intense Pulsed Laser Plasmas. *J. Mater. Res.* **2013**, *28*, 87–93.
- (31) Ishimaru, M.; Zhang, Y.; Shannon, S.; Weber, W. J. Origin of Radiation Tolerance in 3C–SiC with Nanolayered Planar Defects. *Appl. Phys. Lett.* **2013**, *103*, No. 033104.
- (32) Sadow, S. E. *Silicon Carbide Biotechnology: A Biocompatible Semiconductor for Advanced Biomedical Devices and Applications*; Elsevier, 2012.
- (33) Oliveros, A.; Guiseppi-Elie, A.; Sadow, S. E. Silicon Carbide: A Versatile Material for Biosensor Applications. *Biomed. Microdevices* **2013**, *15*, 353–368.
- (34) Zhuang, H.; Yang, N.; Zhang, L.; Fuchs, R.; Jiang, X. Electrochemical Properties and Applications of Nanocrystalline, Microcrystalline, and Epitaxial Cubic Silicon Carbide Films. *ACS Appl. Mater. Interfaces* **2015**, *7*, 10886–10895.
- (35) Yang, N.; Zhuang, H.; Hoffmann, R.; Smirnov, W.; Hees, J.; Jiang, X.; Nebel, C. E. Nanocrystalline 3C–SiC Electrode for Biosensing Applications. *Anal. Chem.* **2011**, *83*, 5827–5830.
- (36) Diaz-Botia, C. A.; Luna, L. E.; Neely, R. M.; Chamanzar, M.; Carraro, C.; Carmena, J. M.; Sabes, P. N.; Maboudian, R.; Maharbiz, M. M. A Silicon Carbide Array for Electrooculography and Peripheral Nerve Recording. *J. Neural Eng.* **2017**, *14*, No. 056006.
- (37) Deku, F.; Cohen, Y.; Joshi-Imre, A.; Kanneganti, A.; Gardner, T. J.; Cogan, S. F. Amorphous Silicon Carbide Ultramicroelectrode Arrays for Neural Stimulation and Recording. *J. Neural Eng.* **2018**, *15*, No. 016007.
- (38) Bernardin, E.; Frewin, C.; Everly, R.; Ul Hassan, J.; Sadow, S. Demonstration of a Robust all-Silicon-Carbide Intracortical Neural Interface. *Micromachines* **2018**, *9*, 412.
- (39) Beygi, M.; Bentley, J. T.; Frewin, C. L.; Kuliasha, C. A.; Takshi, A.; Bernardin, E. K.; La Via, F.; Sadow, S. E. Fabrication of a Monolithic Implantable Neural Interface from Cubic Silicon Carbide. *Micromachines* **2019**, *10*, 430.
- (40) Tanner, P.; Iacopi, A.; Phan, H. P.; Dimitrijević, S.; Hold, L.; Chaik, K.; Walker, G.; Dao, D. V.; Nguyen, N. T. Excellent Rectifying Properties of the *n*-3C–SiC/*p*-Si Heterojunction Subjected to High Temperature Annealing for Electronics, MEMS, And LED Applications. *Sci. Rep.* **2017**, *7*, 17734.
- (41) Wang, L.; Dimitrijević, S.; Han, J.; Iacopi, A.; Hold, L.; Tanner, P.; Harrison, H. B. Growth of 3C–SiC on 150-mm Si (100) Substrates by Alternating Supply Epitaxy at 1000°C. *Thin Solid Films* **2011**, *519*, 6443–6446.
- (42) Phan, H. P.; Dao, D. V.; Nakamura, K.; Dimitrijević, S.; Nguyen, N. T. The Piezoresistive Effect of SiC for MEMS Sensors at High Temperatures: A Review. *J. Microelectromech. Syst.* **2015**, *24*, 1663–1677.
- (43) Maboudian, R.; Carraro, C.; Senesky, D. G.; Roper, C. S. Advances in Silicon Carbide Science & Technology at the Micro and Nano Scales. *J. Vac. Sci. Technol., A* **2013**, *31*, 050805–1.
- (44) Dagdeviren, C.; Hwang, S. W.; Su, Y.; Kim, S.; Cheng, H.; Gur, O.; Haney, R.; Omenetto, F. G.; Huang, Y.; Rogers, J. A. Transient, Biocompatible Electronics and Energy Harvesters based on ZnO. *Small* **2013**, *9*, 3398–3404.
- (45) Song, E.; Li, R.; Jin, X.; Du, H.; Huang, Y.; Zhang, J.; Xia, Y.; Fang, H.; Lee, Y. K.; Yu, K. J.; Chang, J. K.; Mei, Y.; Alam, M. A.; Huang, Y.; Rogers, J. A. Ultrathin Trilayer Assemblies as Long-Lived Barriers Against Water and Ion Penetration in Flexible Bioelectronic Systems. *ACS Nano* **2018**, *12*, 10317–10326.
- (46) Seo, K. J.; Qiang, Y.; Bilgin, I.; Kar, S.; Vinegoni, C.; Weissleder, R.; Fang, H. Transparent Electrophysiology Microelectrodes and Interconnects from Metal Nanomesh. *ACS Nano* **2017**, *11*, 4365–4372.
- (47) Phan, H. P.; Viet Dao, D.; Tanner, P.; Wang, L.; Nguyen, N. T.; Zhu, Y.; Dimitrijević, S. Fundamental Piezoresistive Coefficients of *p*-type Single Crystalline 3C–SiC. *Appl. Phys. Lett.* **2014**, *104*, 111905.
- (48) Dinh, T.; Phan, H. P.; Kashaninejad, N.; Nguyen, T. K.; Dao, D. V.; Nguyen, N. T. An On-Chip SiC MEMS Device with Integrated Heating, Sensing, and Microfluidic Cooling Systems. *Adv. Mater. Interfaces* **2018**, *5*, 1800764.
- (49) Dinh, T.; Phan, H. P.; Qamar, A.; Woodfield, P.; Nguyen, N. T.; Dao, D. V. Thermoresistive Effect for Advanced Thermal Sensors: Fundamentals, Design Considerations, and Applications. *J. Microelectromech. Syst.* **2017**, *26*, 966–986.